MRS Advances (2024) 9:1548–1553
https://doi.org/10.1557/s43580-024-00956-4

ORIGINAL PAPER

Interactions in GO/P3HT thin films: Spectroscopic investigation for organic solar cells

Fokotsa V. Molefe[1,2] · Bakang M. Mothudi[1,2] · Mokhotjwa S. Dhlamini[2] · Mmantsae Diale[1]

Received: 7 June 2024 / Accepted: 2 October 2024 / Published online: 2 December 2024

Abstract

The present study was carried out to investigate the thin film properties of poly (3-hexylthiophene) (P3HT) coupled with graphene oxide (GO) using different spectroscopic techniques. The X-ray diffraction spectrum of GO/P3HT revealed a highly crystalline reflection of GO which is slightly shifted to higher diffraction angles as evidence of interaction with P3HT. Fourier transform infrared confirmed the alteration of P3HT structure upon interaction with GO by the increase in average conjugation length. The reflectance spectrum of GO/P3HT has an observable decrease in percentage reflectance, leading to an enhancement of light absorption. The fluorescent decay curves revealed a decline in exciton lifetime depicting quicker charge transfer, which decreased the exciton diffusion length. Our findings suggest that GO can be the hole transport material in organic solar cells.

Introduction

Currently, photovoltaic (PV) devices are a more viable and promising non-polluting way of generating electricity with the potential to replace conventional fossil fuels. The use of graphene has grown for the past decade as a superstar nanomaterial for tackling energy challenges [1]. It is widely used i.e. field-effect transistors (FETs), transparent electrodes (TEs) and optoelectronic devices [2, 3]. It possesses remarkable characteristics like high specific surface area (theoretically 2630 m^2/g for single-layer-layer graphene), electron transport capabilities and extraordinary electronic properties as well as high thermal conductivity (~5000 Wm^{-1} K^{-1}) [3, 4]. This, in turn, gave graphene derivatives i.e. GO and reduced graphene oxide (rGO) tremendous attention owing to shared properties [5, 6]. The most crucial factors to be considered for proficient OSC devices include strong optical absorption, semitransparency, flexibility and the energy gap between the highest occupied molecular orbital (HOMO) and lowest unoccupied molecular orbital (LUMO) [7, 8]. The increase in optical absorption capacity and the reduction in band gap (E_g) energy help to enhance solar light harvesting. Moreover, luminescence characteristics provide valuable optical information such as charge mobility, lifetime kinetics and carrier recombination [9]. Luminescent materials absorb light in a particular spectral region, store it as energy and re-emit it over time by matching the response of an OSC device thereby improving the absorption and increasing the efficiency [10].

GO's ability to form composites with semiconducting polymers produces excellent optical properties and alleviates efficient charge transfer with reduced recombination losses. The ionic interaction between nanomaterials and organic conjugated polymers improves optoelectronic properties making it well-suited for OSC applications. The properties of GO nanostructures rely mainly on physical and chemical methods wherein the top-down and bottom-up approaches for preparation are followed [6]. GO has been achieved using microwave [11], mechanical exfoliation from graphite [12] and chemical exfoliation also called Hummer's method [13]. Mechanical exfoliation is an easy method, although the yield is quite small, it is difficult to obtain high-quality industrial production. Hummer's method is the top-down approach used in this study because of the benefits like cost-effectiveness, big scale and high yield. It improves the dispersion stability of the produced GO and is environmentally friendly, with no surface flaws [4].

GO has been widely studied for functionalisation using conjugated polymers based on π–π* interactions between

✉ Mmantsae Diale
mmantsae.diale@up.ac.za

[1] Department of Physics, University of Pretoria, Private Bag X 20, Hatfield 0028, South Africa

[2] Department of Physics, University of South Africa, Private Bag X 90, Florida 1710, South Africa

them [14]. The oxygen-containing functional groups in GO i.e. hydroxyl (–OH), carboxylic (-COOH), epoxy (C–O–C) etc.) facilitate chemical functionalisation and bring solubility for film production through solution processes such as layer-by-layer self-assembling [14, 15]. However, functionalization of GO with most polymers presents challenges such as aggregation and poor compatibility due to strong van der Waals forces which reduce their surface energy [16]. Defects and oxygen-containing functional groups primarily act as charge carrier traps, obstructing efficient charge transportation and increasing charge recombination rates [17]. Furthermore, carbon atoms of GO are chemically stable resulting in weak interactions which do not provide efficient load transfer across the interface [18]. To achieve good optical properties, it is deemed important to functionalize the surface of GO. It is widely known that P3HT-derived thiophene derivatives are high-hole mobility materials with substantial electron delocalisation along the chemical backbone. Thus, fine-tuning the work function (WF) of GO by incorporating P3HT can improve optical properties, and photovoltaic parameters of OSC devices due to increased charge carrier mobility [19].

To tackle the limitations, GO and P3HT have been used to grow thin films to improve optical properties. The present work reports on interface interaction between GO and P3HT using spectroscopic techniques. GO is used as the hole transport layer to modify the interface and extract photogenerated charges thus minimising recombination. These findings clarify the nature of the interaction between GO and P3HT and create perspectives for OSCs.

Material and methods

Materials preparation and deposition

The graphite powder (99%), potassium permanganate ($KMnO_4$) (98%), sulphuric acid (H_2SO_4) (98%), hydrogen peroxide (H_2O_2) (30%), phosphoric acid (H_3PO_4), chlorobenzene (99%) and P3HT (99%), respectively, were purchased from Sigma Aldrich (South Africa) and were used as received without additional purification. The amorphous soda-lime non-conducting glass substrates with dimensions 20 × 20 × 2 mm purchased from the Laboratory Consumable Company in South Africa were used for the deposition of thin films. It was preferred owing to its amorphous nature, low heat and chemical resistance allowing the deposition of materials without any interactions that would lead to a common fermi level.

GO sheets were prepared using the modified Hummers method [20]. To create a 5% concentration solution, P3HT was dispersed in chlorobenzene. The solution was agitated for 10 min on a magnetic hot plate with an ambient temperature of 80 °C. The temperature was lowered to 50 °C, while the solution was constantly stirred for 1 h, then cooled at room temperature. The resulting orange suspension was used to grow thin films. The 20 × 20 × 2 mm soda-lime glass substrates were cleaned inside an ultrasonic bath sequentially using acetone, ethanol and deionized (DI) water for 10 min each. The substrates were then dried at 50℃ in an oven followed by UV-ozone treatment for 5 min before spin-coating. A micropipette was used to extract 50 µl of GO and P3HT solution for spin-coating. GO solution was spin-coated at 1400 rpm for 1 min on a glass substrate, while P3HT solution was spin-coated at 800 rpm for 50 s on a bare glass substrate and a GO-coated substrate. After coating, the P3HT and GO/P3HT thin films were soft annealed for 5 min at 100 °C on a hot plate to remove residual solvents.

Materials characterization

The crystalline phases were identified using a Rigaku Smart Lab XRD with CuKα (1.5418 Å) radiation. The Fourier transform infrared (FTIR) spectra were acquired using a SHIMADZU-IRTracer-100 PerkinElmer spectrometer with a resolution of 4.0 cm^{-1} and 10 scans. The optical studies were conducted by a PerkinElmer Lambda spectrometer, model 1050 UV/VIS/NIR. The time-resolved photoluminescence (TRPL) was probed using a 400 nm pulsed laser and the response was captured using time-correlated single photon counting (TCSPC), Model: F980 methodology, Edinburgh Instrument. The instrument response function (IRF) was < 100 ps.

Results and discussion

XRD analysis

The XRD diffractograms of thin films are presented in Fig. 1. The pristine P3HT possesses two diffraction peaks at positions ~ 5.8° and ~ 21° comparable to (100) and (010) orientations of the P3HT polymer with interlayer spacing formed by parallel stacks of main chains [21]. The (100) diffraction corresponds to the a-axis orientation pointing in the direction of the alkyl chains and the (010) is relatable to the π-stacking direction of the polymer backbones consisting of poly-thiophene called b-axis [22, 23]. The presence of these peaks indicates the crystallinity of the polymer within the lamella structure of thiophene rings in P3HT [24]. Several research groups indicated that P3HT has a semicrystalline structure (i.e. amorphous and crystalline) with the crystalline consisting of planar backbones stacked on top of each other [25, 26].

The (001) diffraction peak of GO in GO/P3HT thin film nanocomposite is not noticeable at ~ 11° owing to the small

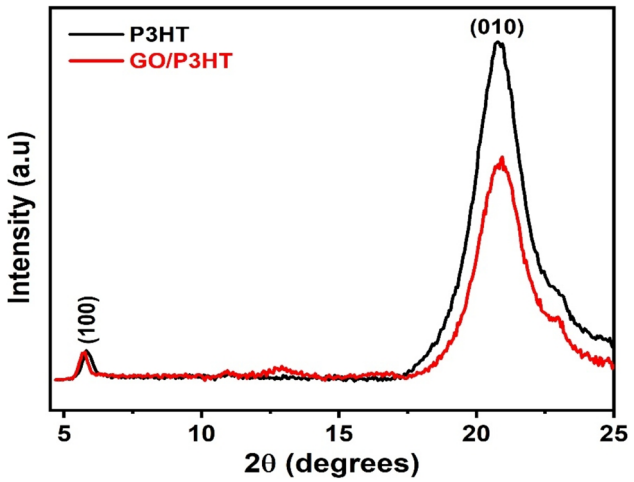

Fig. 1 The XRD patterns of P3HT and GO/P3HT thin films

concentration used. It is evident through (010) diffraction that GO reduced the crystallinity of P3HT. Moreover, the graphitic defects during functionalization with GO slightly shifted those diffraction peaks to lower angles due to the increase in interlayer spacing. Monika et al. investigated the effect of GO on PEDOT:PSS conducting polymers and witnessed a shift to the lower diffraction angle when incorporating GO [27].

FTIR analysis

The linkage at the interface of GO/P3HT was analysed using FTIR as shown in Fig. 2. P3HT presents primary bands ~ 2960, ~ 2925 and ~ 2855 cm^{-1} symbolic of aliphatic C-H stretching of P3HT. The absorption band at ~ 2960 cm^{-1} corresponds to the -CH_3 asymmetry stretch vibration, while bands at ~ 2925 and ~ 2855 represent -CH_2 stretch vibration [25]. The spectra further show a band at ~ 1462 cm^{-1} related to the bending vibration of the C-H bond and the band at ~ 1510 cm^{-1} is associated with asymmetric C = C ring stretching vibrations. The ~ 1378 cm^{-1} C-H vibration band may be due to partial decomposition of the thiophene [28]. Detailed evaluation of GO/P3HT reveals the emergence of vibrational bands at ~ 3372, ~ 3194 and ~ 1081 cm^{-1} which are characteristic of contribution from GO. The C-O stretching vibration at ~ 1081 cm^{-1} affirms the existence of oxide functional groups [29]. The GO/P3HT reveals a band at ~ 1648 cm^{-1} associated with amide carbonyl stretching mode also called Amide I vibrational stretch ν(C = O) [30]. These variations indicate that interactions between GO and P3HT lead to the derivatization of the edge carboxyl and surface hydroxyl functional groups via the formation of amides [29]. The vibration band at ~ 821 cm^{-1} corresponds to aromatic out-of-plain vibration, and it is characteristic of (3-hexylthiophene) which indicates the structure of P3HT contains rr-P3HT chains [14]. The band at ~ 721 cm^{-1} represents methyl rock mode and the CH_3 rocking vibration.

The structural alteration was examined using the ratio of peaks (I_{1510}/I_{1462}) from which the average conjugation length of P3HT increased as the ratio decreased from ~ 1.20 to ~ 1.12 for GO/P3HT. According to Fuentes-Perez et al. [31], the intensity ratio of the C = C symmetric ring stretching to the C = C asymmetric ring stretching (I_{sym}/I_{asym}) is declarative of the conjugation length in the polymer backbone and the smaller values of the ratio I_{sym}/I_{asym} correspond to greater conjugation. They reported reduced conjugation length of P3HT upon incorporating Fe_3O_4 and Fe_3O_4@ $ZnFe_2O_4$ nanocomposites in the polymer matrix. However,

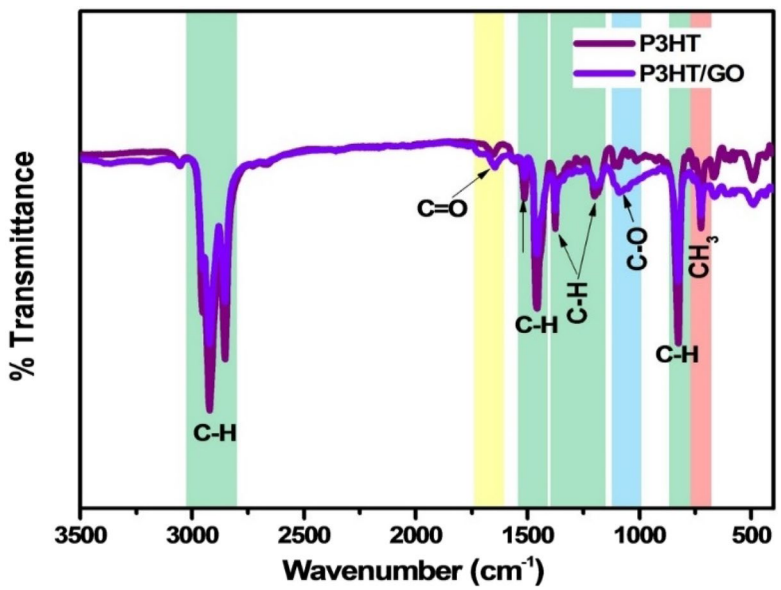

Fig. 2 FTIR spectra of P3HT and GO/P3HT thin films

we attained an increased conjugation length corresponding to the reordering of the polymer backbone. The conjugation length increase supports the XRD results whereby an increase in interlayer spacing was witnessed. Kaur et al. reported a similar substantial reduction in the intensity of prominent bands while modifying P3HT using swift heavy ions [32]. In accord, the intensity ratio was reduced from 7.4 to 6.9 and 5.9 and they ascribed it to the increase in conjugation length. According to Shyam et al. [33], blending an optimum amount of exfoliated C_3N_5 sheets into the P3HT matrix improves the molecular ordering, and structural coherence thereby extending the π-conjugation length in the hybrid thin film and producing excellent device performance.

UV/VIS/NIR analysis

Figure 3 shows the reflectance spectra of the thin films. P3HT has an absorption edge below 600 nm with the highest % reflectance of ~ 97%. The absorption edge of GO/P3HT is redshifted in association with sufficiently increased chain motion, which indicates an increase in the crystalline ordering that caused the stabilization of the P3HT chains [34]. Li et al. [35] ascribed the redshift to enhancement of the light absorption capability of P3HT upon interaction with GO. Other researchers noticed no remarkable difference when incorporating GO in a polyaniline hybrid system (PANI-base-GOX) except for the redshift in absorption peaks due to the interaction which indicates a decrease in an optical E_g for the composite films [36]. In another study, a 2 to 3% decrease in % transmittance was recorded in PEDOT:PSS:GO composite thin film due to the absorption of GO [37]. For GO/P3HT, the absorption band is a bit stronger symbolized by a decrease in % reflectance. The observed stronger absorption is attributed to the π-π* transition at the GO/P3HT interface [38]. This is due to the improvement in the chain segments' effective conjugation lengths in the P3HT backbone, which more closely localizes the exciton wave function and raises its energy [39]. The undertaken interaction is linked to inter-chain order (a rise in P3HT chains' disorder), which improves absorption [40]. Ren et al. [41] associated the stronger vibronic absorption of P3HT:5CB nanocomposite with the enhanced conjugation length of the backbone. The nanocomposite comprising few-layered graphene (FLG) with P3HT (P3HT/FLG) demonstrated the improvement in light absorption favouring electronic transitions graphene adds and facilitating charge mobility while reducing potential barrier [42]. They noted that FLG tends to increase E_g by 0.1 eV and improve energy conversion efficiency due to improved exciton dissociation as a known effect of electron acceptors.

TRPL analysis

The TCSPC photoluminescence decays of thin films acquired at an excitation wavelength of 400 nm while monitoring emission at 600 nm are shown in Fig. 4. The fluorescence decay of the films was analysed by fitting data to a third-order exponential function shown in Eq. (1) [43] from the instrument analysis software:

$$I(t) = I_o e^{-(t/\tau_1)} + I_o e^{-(t/\tau_2)} + I_o e^{-(t/\tau_3)}, \quad (1)$$

where $I(t)$ is the fluorescence intensity at time t, I_0 is the initial fluorescence intensity, and τ represents a lifetime.

The decay curve of P3HT showed an exciton lifetime of ~ 0.872 ns from un-adhered P3HT molecules. GO/P3HT revealed a shorter lifetime of ~ 0.635 ns. The reduction in the lifetime indicates exciton dissociation before emission thus promoting faster charge transfer. The shortened

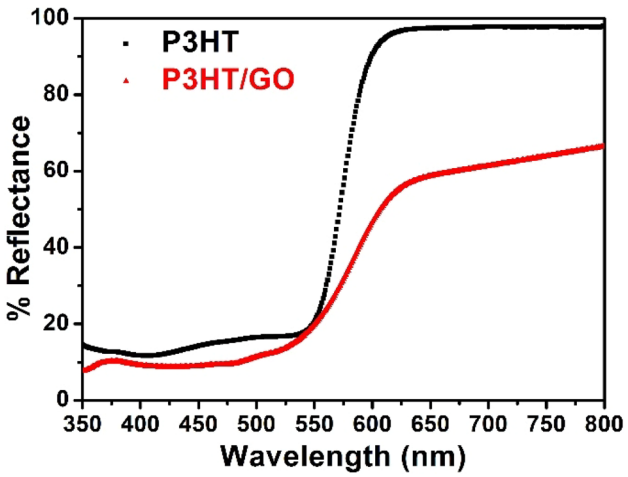

Fig. 3 Diffuse reflectance spectra of P3HT and GO/P3HT thin films

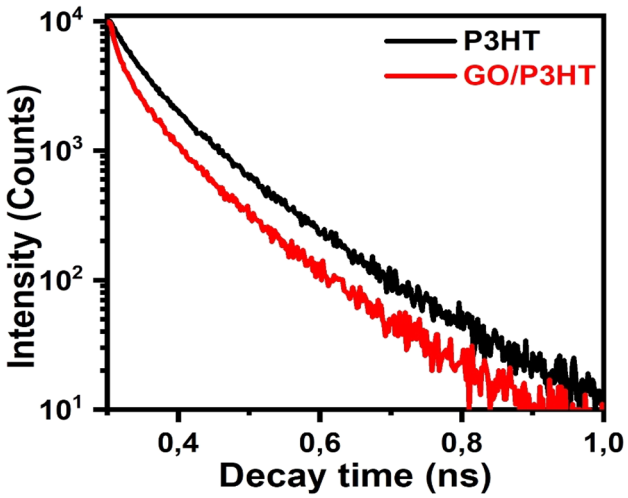

Fig. 4 PL decay curves of P3HT and GO/P3HT thin films

lifetime is assigned to the existence of an extra non-radiative decay pathway due to charge transfer [44]. This agrees with the results of Zheng et al. [45]. Our results corroborated the findings of Ren et al. [46], who noticed more rapid fluorescence decay of P3HT/graphene insinuating direct charge transfer at the interface resulting in higher photocurrent of polymer solar cells. GO as a charge carrier extractor in g-C_3N_4 electrospun on polyvinyl difluoride (PVDF) increased the average lifetime of photogenerated charge carriers from 4.63 to 5.2 ns associated with improved electron–hole separation efficiency. [47]. The PL decay kinetics conducted on GO-PANI produced an increased lifetime from 2.1 to 3.0 ns due to the more effective interaction of GO moiety with PANI through functional groups [48]. From the obtained lifetime, we estimated the exciton diffusion length of the thin films using Eq. (2) to get more insight into their conformation [49]:

$$L_D = \sqrt{D \times \tau}, \tag{2}$$

where τ is the exciton lifetime and D is the diffusion constant ($D = 1.8 \times 10^{-7} m^2.s^{-1}$). The diffusion lengths are ~ 12.5 and ~ 10.7 nm for P3HT and GO/P3HT, respectively.

Conclusion

It was feasible to generate P3HT and GO/P3HT thin films using a spin coater. We discovered that the structural, and optical features of P3HT were affected during interaction with GO. FTIR confirmed the interaction via the prevalence of oxygen-containing groups and the reduction of C-H bands. The observed redshift denotes the improvement of light absorption. The reduced lifetime of GO/P3HT suggests that the photoinduced charge transfer took place at the interface. This charge transfer symbolised by the fast decay of GO/P3HT is highly favoured for efficient OSCs.

Acknowledgments The authors are grateful for financial support from NRF grant no. 94951 and grant holder-linked postdoctoral fellowships and staff development grants no. 115463.

Author contributions Fokotsa V. Molefe conceived and designed the experiments, performed the experiments, analysed and interpreted the data, and wrote the paper. Bakang M. Mothudi contributed reagents; materials and analysis tools. Mkhotjwa S. Dhlamini contributed towards supervision, administration, conceived and designed the experiments, contributed reagents, materials, analysis tools review and editing. Mmantsae Diale contributed towards Supervision, review and editing, and funding acquisition.

Funding Open access funding provided by University of Pretoria.

Data availability Data will be made available on request.

Declarations

Competing interest The authors declare that they have no known competing financial interests or personal relationships that could have appeared to influence the work reported in this paper.

References

1. K.S. Novoselov, A.K. Geim, S.V. Morozov, D. Jiang, Y. Zhang, S.V. Dubonos, I.V. Grigorieva, A.A. Firsov, Science **306**, 666–669 (2004)
2. T. Enoki, Carbon **49**, 2579 (2011)
3. T. Lim, C.S. Kim, M. Song, S.Y. Ryu, S. Ju, Synth. Met. **205**, 1–5 (2015)
4. J. Song, X. Wang, C. Chang, J. Nanomater. (2014). https://doi.org/10.1155/2014/276143
5. C.K. Chua, M. Pumera, Chem. Soc. Rev. **43**, 291–312 (2014)
6. B. Li, Y. Nan, P. Zhang, Z. Wang, Q. Lu, X. Song, Diamond Relat. Mater. **55**, 87–94 (2015)
7. Z. Ali, S. Abdalla, E.A. Hassan, Y. Umar, M.M. Al-Mogren, Mater. Today Commun. **32**, 104048 (2022)
8. I. Shafiq, M. Khalid, M. Muneer, M.A. Asghar, R. Baby, S. Ahmed, T. Ahamad, S.F.A. Morais, A.A.C. Braga, Mater. Chem. Phys. **308**, 128154 (2023)
9. H. Guo, X. Wang, M. Zhang, T. Pullerits, P. Song, Spectrochim. Acta Part A Mol. Biomol. Spectrosc. **325**, 125058 (2025)
10. T. Sharma, T.T.H. Nguyen, N.H. Nguyen, H.L. Ngo, Y.H. Soo, C.Y. Ng, H.K. Jun, Heliyon **10**, e26048 (2024)
11. N. Kim, G. Xin, S.M. Cho, C. Pang, H. Chae, Curr. Appl. Phys. **15**, 953–957 (2015)
12. X.C. Dong, D.L. Fu, W.J. Fang, Y.M. Shi, P. Chen, L.J. Li, Small **5**, 1422 (2009)
13. S. Park, R.S. Ruoff, Nat. Nanotechnol. **4**, 217 (2009)
14. D. Yu, S.Y. Yang, M. Durstock, J.B. Baek, L.M. Dai, ACS Nano **4**, 5633–5640 (2010)
15. Y. Liu, D. Yu, C. Zeng, Z. Miao, L. Dai, Langmuir **29**, 6158–6160 (2010)
16. M. Zafar, S.M. Imran, I. Iqbal, M. Azeem, S. Chaudhary, S. Ahmad, W.Y. Kim, Results Phys. **60**, 107655 (2024)
17. I.N. Reddy, B. Akkinepally, J. Shim, C. Bai, Micromachines **15**, 1125 (2024)
18. C. Guarda, B. Faria, J.N.C. Lopes, N. Silvestre, Compos. Sci. Technol. **250**, 110514 (2024)
19. F.V. Molefe, M. Khenfouch, M.S. Dhlamini, B.M. Mothudi, Adv. Mater. Lett. **8**, 246–250 (2017)
20. F.V. Molefe, B.M. Mothudi, M.S. Dhlamini, Results Opt. **16**, 100684 (2024)
21. M. Shukla, A. Tiwari, J. Agrawal, A. Bilgaiyan, V. Singh, Phys. E **115**, 113694 (2020)

22. T. Sharma, R. Singhal, R. Vishnoi, G.D. Sharma, S.K. Biswas, Phys. B **537**, 306–313 (2018)
23. R.K. Pandey, H. Bisht, S.K. Yadav, A.K. Singh, R. Prakash, Mater. Sci. Eng. B **260**, 114622 (2020)
24. M.M. Stylianakis, E. Stratakis, E. Koudoumas, E. Kymakis, S.H. Anastasiadis, A.C.S. Appl, Mater. Interfaces **4**, 4864–4870 (2012)
25. F.V. Molefe, M. Hamzah, M. Khenfouch, M.S. Dhlamini, B.M. Mothudi, J. Phys. Conf. Ser. **984**, 012003 (2018)
26. J.A. Lim, F. Liu, S. Ferdous, M. Muthukumar, A.L. Briseno, Polymer semiconductor crystals. Mater. Today **13**, 14–24 (2010)
27. P. Monika, V. Pradhan, A.C. Amrute, Mater. Today Proceed. (2023). https://doi.org/10.1016/j.matpr.2023.07.123
28. P. Kovacik, O. College, *Vacuum deposition of organic molecules* (University of Oxford, Oxford, 2011)
29. F.Y. Ban, S.R. Majid, N.M. Huang, H.N. Lim, Int. J. Electrochem. Sci. **7**, 4345–4351 (2012)
30. D. Romero-Borja, J.-L. Maldonado, O. Barbosa-García, M. Rodríguez, E. Pérez-Gutiérrez, R. Fuentes-Ramírez, G. de la Rosa, Synth. Met. **200**, 91–98 (2015)
31. M. Fuentes-Perez, P. Acevedo-Pena, M.A. Ramírez-Gomez, J.A. Alanís-Navarro, M.E. Nicho, Synth. Met. **299**, 117456 (2023)
32. A. Kaur, A. Dhillon, G.B.V.S. Lakshmi, Y. Mishra, D.K. Avasthi, Mater. Chem. Phys. **131**, 436–442 (2011)
33. R. Shyam, S. Jana, T. Manaka, R. Prakash, Sens. Actuators: B Chem. **418**, 136190 (2024)
34. T. Erb, U. Zhokhavets, G. Gobsch, S. Raleva, B. Stuhn, P. Schilinsky, C. Waldauf, C.J. Brabec, Adv. Funct. Mater. **15**, 1193–1196 (2005)
35. G. Li, V. Shrotriya, J. Huang et al., Nat. Mater. **4**, 864–868 (2005)
36. F.F. Sead, E.H. Sahap, N.A.-S. Ridha, H.K. Egzar, H.N. Abed, R.M. Thyab, W.I. Yahya, I. Alrubaie, Opt. Mater. **150**, 115254 (2024)
37. R.K. Sharma, D. Sharma, A. Saini, S. Laxmi, B.P. Singh, S.K. Srivastava, Mater. Today: Proceed. **82**, 375–380 (2023)
38. V. Shrotriya, J. Ouyang, R.J. Tseng, G. Li, Y. Yang, Chem. Phys. Lett. **411**, 138–143 (2005)
39. P.J. Brown, D.S. Thomas, A. Köhler, J.S. Wilson, J.-S. Kim, C.M. Ramsdale, H. Sirringhaus, R.H. Friend, Phys. Rev. B **67**, 1–16 (2003)
40. J. Arranz-Andrés, W.J. Blau, Carbon **46**, 2067–2075 (2008)
41. W. Ren, S. Li, J. Ren, Y. Liu, Y. Wu, Q. Sun, Y. Cui, Y. Hao, Chem. Eng. J. **455**, 140831 (2023)
42. L.G.P. Tienne, T.P. Paula, M.F.V. Marques, Mater. Sci. Eng. B **293**, 116505 (2023)
43. S.J. Mofokeng, L.L. Noto, R.E. Kroon, O.M. Ntwaeaborwa, M.S. Dhlamini, J. Lumin. **223**, 117192 (2020)
44. F. Zheng, X.Y. Yang, P.Q. Bi, M.S. Niu, C.K. Lv, L. Feng, W. Qin, Y.Z. Wang, X.T. Hao, K.P. Ghiggino, Org. Electron. **44**, 149–158 (2017)
45. F. Zheng, W.L. Xu, X.T. Han-Dong Jin, K.P.G. Hao, RSC Adv. **5**, 89515–89520 (2015)
46. L. Ren, J. Qiu, S. Wang, Compos.: Part B **55**, 548–557 (2013)
47. Z. Vilamova, P. Czernek, J. Zagora, L. Svoboda, J. Bednar, Z. Simonova, D. Placha, R. Dvorsky, Appl. Surf. Sci. **677**, 161055 (2024)
48. D.K. Pyne, S. Chatterjee, S. Pramanik, A. Halder, Mater. Chem. Phys. **318**, 129241 (2024)
49. G.L. Kabongo, P.S. Mbule, G.H. Mhlongo, B.M. Mothudi, M.S. Dhlamini, Bull. Mater. Sci. **43**, 48 (2020)